Comprehensive Reliability Analysis of Fractional Frequency Offshore Wind Power Systems Considering Environmental Impact and Overall Structure: a Case Study in China

Zhongqi Cai, Chengxiao Wei, Sui Peng, and Xiuli Wang

***Abstract*—The rapid expansion of offshore wind power plays a crucial role in China's pursuit of its 'dual carbon goals'. Fractional frequency transmission, an emerging technology for delivering large-scale offshore wind power, currently lacks extensive research attention. This paper addresses this gap by proposing a reliability assessment model for fractional frequency systems, encompassing generation, boosting, transmission, and conversion processes. Additionally, the study conducts a quantitative analysis of severe weather impacts on offshore component maintenance. With a focus on China's offshore wind power development, the research includes comparative analyses of various offshore regions, system topologies, and transmission methods to evaluate system reliability. This comprehensive analysis serves as a valuable reference for the strategic planning and large-scale deployment of grid-connected offshore wind power systems.**

***Index Terms*—Fractional frequency transmission system, offshore wind power, reliability assessment, environmental impact.**

NOMENCLATURE

A. Abbreviations

HVAC	high-voltage AC transmission
HVDC	high-voltage DC transmission
FFTS	fractional frequency transmission system
M3C	modular multilevel matric converter
SM	sub-module
IGBT	insulate-gate bipolar transistor
MTTF	mean time to failure
MMC	modular multilevel converter

B. Variables

V_{ij}^{*}	wind speed of the turbine at row i and column j considering the effect of multiple wind turbines
V_{ij}	wind speed at row i and column j considering single turbine wake effects
V_0	initial wind speed of the wind farm
N_{row}	total rows of wind farm
N_{col}	total columns of wind farm
S_{ij}	area of overlap with the wind turbine wake at row i, column j
S	area of the turbine
P_{PZ1}	exact probability of "first-order protection zone failure"
P_{PZ1}^{0}	probability of "non circuit breaker failure in the protection zone"
P_{PZ1}^{*}	probability of "all circuit breakers and components outside the protection zone are working"
p_{c}	probability of single collection cable working properly
p_{b}	probability of single breaker working properly
N_{c}	total number of collection cables
N_{b}	total number of breakers
x_{s}	fault state number of collection system
n_{s}	total number of fault states
λ_{SM}	failure rate of SM
λ_{IGBT}	failure rate of IGBT
λ_{cap}	failure rate of capacitor
λ_{SW}	failure rate of switching control module
λ_{arm}	failure rate of bridge arm
λ_{rac}	failure rate of series reactor

Received: March 3, 2024
Accepted: September 21, 2024
Published Online: January 1, 2025

Zhongqi Cai is with the Zhuhai Power Supply Bureau, Guangdong Power Grid Corporation, Zhuhai 519000, China (e-mail: 1035919608@qq.com).

Chengxiao Wei and Xiuli Wang (corresponding author) are with the School of Electrical Engineering, Xi'an Jiaotong University, Xi'an 710049, China (e-mail: weiccx@163.com; xiuliw@mail.xjtu.edu.cn).

Sui Peng is with the Power Grid Planning and Research Center, Guangdong Power Grid Corporation, Guangzhou 510220, China (e-mail: pengsui@gd.csg.cn).

DOI: 10.23919/PCMP.2023.000285

R_{arm}	reliability function for the bridge arm
k	number of SMs in a bridge arm without redundancy
n	number of SMs in a bridge arm considering redundancy
t_{arm}	MTTF of the bridge arm
λ_{M3C}	failure rate of M3C station
λ_{con}	failure rate of control element
A_{M3C}	availability of M3C station
A_{con}	availability of control element
o	output power of FFTS
p_{s}	probability distribution of available capacity for offshore wind systems
p_{w}	normalized turbine output distribution
s	available capacity for offshore wind systems
O	system outage status set
D_i	the number of days required to complete a sub-task i
T^{RH}	operating time required for maintenance
T^{WH}	work time of one working day including travel time
T^{TH}	travel time to the failure site
D_{ns}	non-sailable days during maintenance
λ	severe weather arrival rate
T_i^{R}	mean repair time for task i
A	probability of good weather
μ	repair rate considering severe weather

I. Introduction

In September 2020, Chinese President Xi Jinping announced at the United Nations General Assembly that China aims to peak its carbon dioxide emissions before 2030 and achieve carbon neutrality before 2060. Against this backdrop, the generation of renewable energy, such as wind power, has been increasing. Compared with onshore wind power, offshore wind power has various advantages, such as stable wind energy, no land occupation, and proximity to the consumer market, which makes it suitable for large-scale development with enormous potential. China has abundant offshore wind energy resources [1] with an average annual wind speed of 7–8.5 meters per second at a height of 90 m in most nearshore areas, providing favorable conditions for the construction of large-scale offshore wind farms.

The grid connection difficulty of large-scale offshore wind power is typically higher than that of onshore wind power. Currently, there are three main grid-connection technologies for offshore wind power: high-voltage AC transmission (HVAC), high-voltage DC transmission (HVDC), and fractional frequency transmission systems (FFTS) [2]. The FFTS was first proposed in 1994 for long-distance hydropower development [3]. The FFTS reduces the transmission frequency, shortens the electrical distance of the line, and enhances the transmission capacity, which has the advantage of being more economical and reliable [4]. The FFTS has several practical projects in China and runs well. Among these, the 220 kV Hangzhou flexible low-frequency transmission project in Zhejiang Province has played an experimental role in offshore wind power systems.

Comparing the three transmission methods, the HVAC system has a simple structure, low cost, and rich operation experience; however, with an increase in the transmission distance and capacity, the capacitive charging current increases sharply, and the line loss increases, which is only suitable for the transmission of small-capacity wind power in the near distance. The HVDC system avoids the influence of the capacitive charging current and adopts a modular multilevel converter to reduce the output voltage harmonic content and switching loss. However, it needs to build two converter stations onshore and offshore, which is technically difficult, expensive, and less reliable. In the FFTS system, owing to the frequency reduction, the cable capacitive charging current is significantly reduced compared to that of the HVAC. Unlike HVDC, it only needs to build one converter station onshore. Therefore, FFTS has the advantages of being more economical and reliable and is suitable for large-scale, long-distance offshore wind power transmission [5].

Offshore wind-power systems primarily consist of wind turbines, collection systems, and transmission systems. Owing to the harsh environment, the failure rate and maintenance time of the components are significantly higher than those of onshore wind farms. Additionally, wind power generation exhibits characteristics such as randomness and fluctuations. Large-scale wind power integration causes greater uncertainty in power system planning and is increasingly becoming a major cause of system loss of load risk [6].

However, the reliability analysis of offshore wind power systems faces difficulties. For example, there are many internal components in the converter and the failure mechanism is complicated [7]. The wind farm output and maintenance process are greatly affected by the harsh offshore environment [8]. There is no clear meaning of load in grid connection research on offshore wind power systems, and reliability analysis focuses on studying the level at which offshore wind power systems provide output to the main grid [9], [10]. Currently, there is relatively little research on the grid-connected power capacity of fractional-frequency transmission systems, and there is a lack of detailed system-wide reliability assessments.

Considering the impact of topology and severe weather, this study conducts a comprehensive analysis of a grid-connected offshore wind power system based on a reliability assessment. The main conclusions of this study are as follows:

1) Establishing reliability models for each subsystem of a fractional-frequency offshore wind power system.

2) Impact of severe weather on system reliability.

3) Perform a reliability analysis on case studies to compare the grid integration capacity of offshore wind power in different regions, system topologies, and transmission methods.

The main innovations of this study are as follows:

1) Conducting a system-wide reliability assessment that covers the "generation-collection-transmission-conversion" process.

2) Based on meteorological statistics, we quantitatively analyzes the impact of severe weather on the reliability from the perspective of offshore component maintenance processes.

3) Comprehensively describe reliability in terms of available capacity and output level, considering system reliability and wind resource enrichment.

The remainder of this paper is organized as follows. Section II presents the reliability model of an offshore wind power system. Section III analyses the impact of severe weather conditions. The reliability of the 900 MW offshore wind farm case is evaluated in Section IV. Different sea areas, system topologies, and transmission methods are also compared. Finally, conclusions are presented in Section V.

II. Reliability Model for FFTS

The power system on the fractional side can be divided into subsystems, including a generation system, collection system, boosting station, submarine cables, and a converter station. In this section, a reliability assessment is conducted for these critical subsystems by analyzing their constituent components and structures. Subsequently, the overall system reliability is analyzed.

A. Model of Wind Turbine

In large-scale wind farms, the wake effect is a significant factor contributing to power generation loss [11]. The upstream turbines extract a portion of the wind energy, creating a wake area that reduces the efficiency of the downstream turbines. The closer the proximity between the two turbines, the more pronounces the wake effect. Figure 1 shows a general depiction of the wake impact.

The area of overlap between the wake circle and the downstream turbine is calculated using geometric analysis. Building on the Jensen model, the superposition effect of multiple turbines and incomplete bypassing of the wake are considered to derive the actual wind speed at any given turbine location in a wind farm [12], [13]. The wind speed of the turbine in the row i and column j of the wind farm can be calculated as follows:

$$V_{ij}^{*}=V_0\left[1-\sqrt{\sum_{i=1}^{N_{\text{row}}}\sum_{j=1}^{N_{\text{col}}}\left\{1-\left[\left(\frac{V_{ij}}{V_0}\right)\left(\frac{S_{ij}}{S}\right)\right]^2\right\}}\right] \tag{1}$$

where V_{ij}^{*} is wind speed of the turbine at row i and column j considering the effect of multiple wind turbines; V_{ij} is wind speed considering single turbine wake effects at row i and column j; V_0 is initial wind speed of the wind farm; N_{row}, N_{col} is total rows and columns respectively of wind farm; S_{ij} is area of overlap with the wind turbine wake at row i, column j; S is area of the turbine.

By combining the turbine power curves [14], we derive a turbine power output model that considers the wake effect.

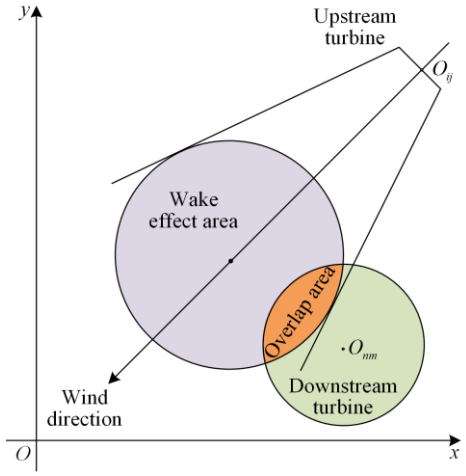

Fig. 1. Influence of wake effects.

B. Model of Collection System

The collection system transports and gathers electricity generated by the wind turbines to the main collection bus. The failure and unavailability rates of components in the collector system are low, but their impact on system reliability is high [15]. Common collection system topologies include linear, large-loop, single-sided, and double-sided loops. Depending on the breaker configuration strategy, collection systems can be classified into three types: conventional, partial, and complete [16], [17].

By analyzing the minimum blackout area as a unit, each unit is referred to as a protection zone, and the fault state of the protection zone reflects the fault state of the collection system. As shown in the Fig. 2, the protection zones form connected regions, and the protection zones are connected by breakers.

When only one protection zone is out-of-operation, it is referred to as a first-order protection zone failure. In this case, the out-of-operation protection zone contains at least one component failure that is not a breaker, whereas the breakers and components outside the faulty zone remain functional. The exact probability of this occurrence is as follows:

$$P_{\text{PZ1}}(i)=P_{\text{PZ1}}^{0}(i)P_{\text{PZ1}}^{*}(i) \tag{2}$$

where P_{PZI} is exact probability of "first-order protection zone failure"; P^{0}_{PZI} is exact probability of "non circuit breaker failure in the protection zone"; P^{*}_{PZI} is exact probability of "all circuit breakers and components outside the protection zone are working"; i is the number of the protected zone where the failure occurred. The values of $P^{0}_{\mathrm{PZI}}(i)$ and $P^{*}_{\mathrm{PZI}}(i)$ are calculated as follows:

$$P^{0}_{\mathrm{PZI}}(i)=\sum_{k=1}^{N_{\mathrm{c},i}}\left(C^{k}_{N_{\mathrm{c},i}}(1-p_{\mathrm{c}})^{k}\,p_{\mathrm{c}}^{N_{\mathrm{c},i}-k}\right) \tag{3}$$

$$P^{*}_{\mathrm{PZI}}(i)=p_{\mathrm{c}}^{N_{\mathrm{c}}-N_{\mathrm{c},i}}\,p_{\mathrm{b}}^{N_{\mathrm{b}}} \tag{4}$$

where p_{c} and p_{b} are the probabilities of a single collection cable and breaker working properly, respectively; $N_{\mathrm{c},i}$ and $N_{\mathrm{b},i}$ is the number of collection cables and breakers in protection zone i; N_{c} and N_{b} is the total number of collection cables and breakers.

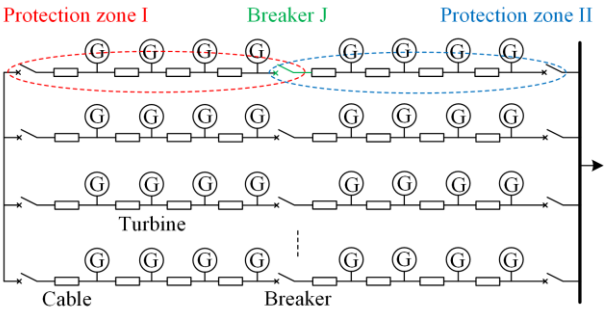

Fig. 2. Schematic of the protection zone.

The analysis method for second-order protection zone failures is similar to that for first-order protection zone failures and will not be elaborated upon here. In practice, the probability of three or more protection zones experiencing simultaneous failures is extremely low. Therefore, only first- and second-order protection zone failures are enumerated and analyzed. Once the status of the upper-level collection system is determined, the reliability models of the various turbine components are simplified and equivalently represented.

In the current fault state, the out-of-operation protection zone and the connected turbines are removed from the original topology, resulting in the topology shown in Fig. 3(a). The turbines shown in the diagram are classified into three categories.

1) Turbines that export power through their own serial cables and do not provide backup for other units.

2) Turbines that cannot export power through their own serial cables and require power transmission through other cables.

3) Turbines whose serial cables are not faulty and provide backup for other units.

To obtain the equivalent turbines G1–G5 shown in Fig. 3(b), the turbines of each category are connected in parallel. The "capacity component" is used to describe the upper limit of the cable's transmission capacity and is connected in series between the main collection bus and the equivalent turbines.

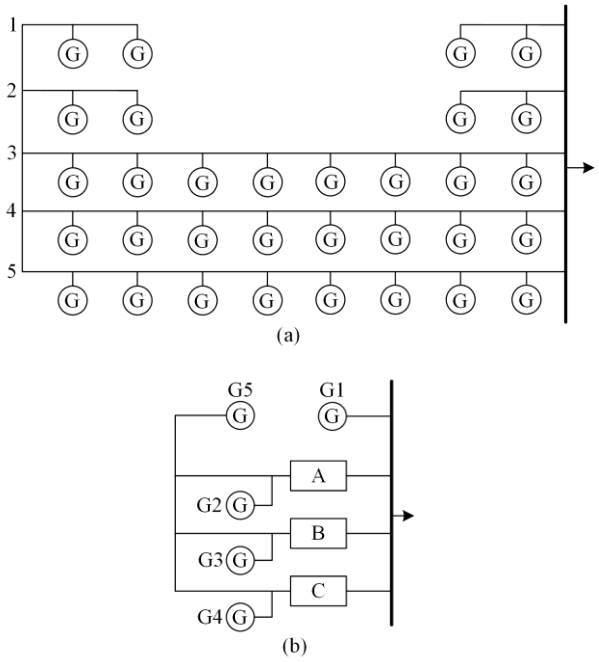

Fig. 3. Simplification and unit equivalence of the collection system. (a) Removal of the faulty zone. (b) Equivalent unit.

By connecting the turbines and capacity components, a simplified fault state of the collection system that no longer contains a loop structure is obtained. The conditional outage table of the system under this fault condition is derived using the series-parallel analysis method.

The fault states of each protection zone are enumerated, an equivalent turbine simplification is employed, and the conditional outage tables for each fault state are calculated. Using the total probability theorem, the overall outage table of the collection system is computed as follows:

$$p(c)=\sum_{x_{\mathrm{s}}=1}^{n_{\mathrm{s}}}p(c\,|\,x_{\mathrm{s}})\,p(x_{\mathrm{s}}) \tag{5}$$

where $p(c\,|\,x_{\mathrm{s}})$ is the probability that the capacity at fault state x_{s} is c; $p(c)$ is the probability that fault state x_{s} occurs; n_{s} is the total number of fault states.

Compared to the simple enumeration assessment of component failure states, the hierarchical analysis of collection system reliability using protection zone models and equivalent turbine models offers several advantages, including reduced fault state space, decreased computational complexity, consideration of a greater number of system states, and higher accuracy.

C. Model of Converter Station

Frequency conversion is the core segment of FFTS, modular multilevel matric converter (M3C) is a kind of AC to AC converter based on fully controlled devices

[18], [19]. M3C has nine bridge arms connecting the two sides of the industrial frequency and fractional frequency systems. It can independently control active and reactive powers, has more flexible and complex switching modes, and its modularized structure makes it suitable for high-voltage and high-power applications.

The topology of the M3C converter is illustrated in Fig. 4. Each bridge arm is composed of several submodules (SMs) in series with a reactor.

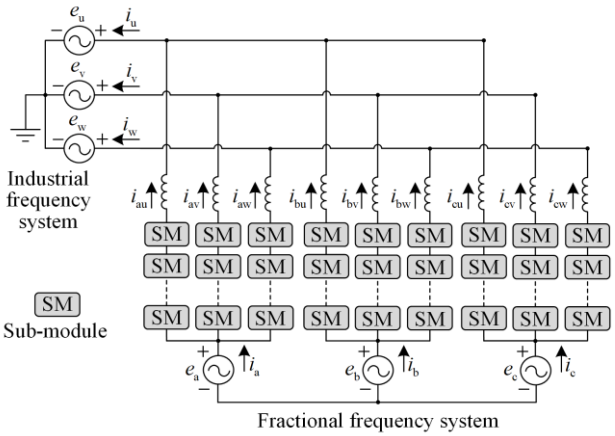

Fig. 4. Topology of M3C.

Redundancy is typically provided to the bridge arm submodules to enhance the reliability of converter stations [20]. The operation of a bridge arm typically requires a minimum number of SMs. When the available number of SMs is greater than the minimum requirement, the bridge arm can function properly [21].

The structure of the full-bridge submodule is illustrated in Fig. 5. One submodule consists of four insulate-gate bipolar transistor (IGBT) modules, capacitors, parallel thyristors, bypass switches, and submodule control drive systems. All components must be in a functional state for the submodule to operate properly.

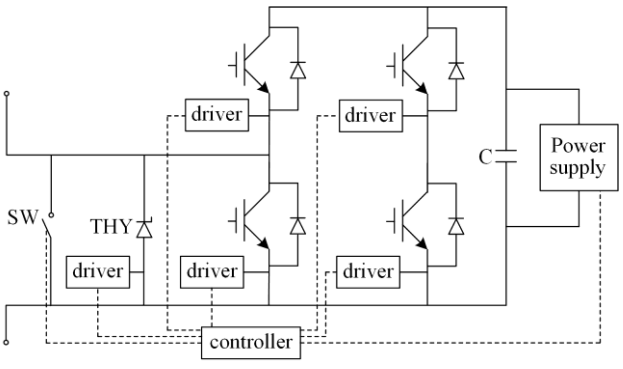

Fig. 5. Structure of the full-bridge SM.

The reliability analysis begins with submodules based on the structural characteristics of the converter. Assuming that the lifetimes of all the components follow an exponential distribution, their failure rates are constant. The full-bridge submodule can be abstracted as a series connection of the IGBTs, capacitors, and switching control modules, as shown in Fig. 6.

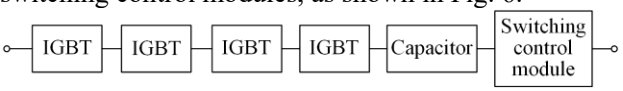

Fig. 6. Reliability diagram of the SM.

The components are connected in series, and the failure rate of the submodules is given by

$$\lambda_{\mathrm{SM}} = 4\lambda_{\mathrm{IGBT}} + \lambda_{\mathrm{cap}} + \lambda_{\mathrm{SW}} \tag{6}$$

where λ_{SM}, λ_{IGBT}, λ_{cap}, and λ_{SW} are the failure rates of the SM, IGBT, capacitor, and switching control modules, respectively.

Without redundancy, the bridge arm consists of a series of k submodules and one reactor. The reliability parameters of the bridge arm are as follows:

$$\lambda_{\mathrm{arm}} = k\lambda_{\mathrm{SM}} + \lambda_{\mathrm{rac}} \tag{7}$$

where λ_{arm} and λ_{rac} are the failure rates of the bridge arm and series reactor, respectively.

Considering the redundancy, we assume that the number of redundant submodules is n. When the bridge arm operates normally, the redundant submodules are not active. They are engaged only as replacements when a submodule fails. This strategy is referred to as the cold-standby strategy for the submodules. The reliability function for the bridge arm with cold-standby, denoted as $R_{\mathrm{arm}}(t)$, can be expressed as:

$$R_{\mathrm{arm}}(t) = \mathrm{e}^{-(k\lambda_{\mathrm{SM}}+\lambda_{\mathrm{rac}})t}\sum_{i=0}^{n}\frac{(k\lambda_{\mathrm{SM}}t)^i}{i!} \tag{8}$$

If the redundant submodules are activated and operate alongside the other submodules in the bridge arm, with any failed submodule automatically removed, it is referred to as the hot-standby strategy for the submodules. The reliability function for the bridge arm with hot standby can be expressed as

$$R_{\mathrm{arm}}(t) = \mathrm{e}^{-\lambda_{\mathrm{rac}}t}\sum_{i=k}^{k+n}C_{k+n}^{i}\mathrm{e}^{-i\lambda_{\mathrm{SM}}t}(1-\mathrm{e}^{-\lambda_{\mathrm{SM}}t})^{n+k-i} \tag{9}$$

In this case, the lifetime of the bridge-arm model no longer follows an exponential distribution. The mean time to failure (MTTF) for the bridge arm can be calculated using the following equation:

$$t_{\mathrm{arm}} = \int_0^{\infty} R_{\mathrm{arm}}(t)\mathrm{d}t \tag{10}$$

The failure rate of the bridge arm is

$$\lambda_{\mathrm{arm}} = \frac{1}{t_{\mathrm{arm}}} \tag{11}$$

In addition to considering the faults of the submodules and other components, the reliability analysis of the converter station also considers the failures of auxiliary systems, such as control protection, valve cooling, power supply, and insulation [22]. By abstracting the aforementioned systems as control elements, the relia-

bility model of the converter station is composed of nine bridge arms in series with one control element. The failure rate and availability of the converter station are expressed as follows:

$$\lambda_{\mathrm{M3C}} = 9\lambda_{\mathrm{arm}} + \lambda_{\mathrm{con}} \tag{12}$$

$$A_{\mathrm{M3C}} = A_{\mathrm{con}} A_{\mathrm{arm}}^{9} \tag{13}$$

where λ_{M3C} and λ_{con} are the failure rates of the M3C station and the control element; A_{M3C} and A_{con} are the availability of the M3C station and the control element.

It should be noted that the topology of the M3C had no influence on the overall reliability assessment process because each subsystem is modeled independently. The M3C used in this study has a 9-bridge arm structure, which is the mainstream topology. If other types of converters are used, such as thyristor-based cycloconverters or hexverters, a reliability model must be established for the internal structure of the converter to obtain the subsystem shutdown table to participate in subsequent full-system calculations [23], [24].

D. Model of Overall System

The main components of an offshore boosting station are parallel transformers and buses. A reasonable simplification can be applied by considering both the transformers and buses as binary elements while retaining their main wiring configuration and disregarding the post-transformer structure for reliability analysis.

The reliability of submarine cables is influenced by various internal and external factors, including material aging, harsh environments, and human activity [25], [26]. This study suggests that the average repair time of submarine cables is approximately linearly correlated with cable length. When the cable length is relatively short, the failure rate remains constant; however, for longer cable lengths, the failure rate exhibits a linear relationship with the cable length. A fitting function is used to describe the reliability parameters of submarine cables [27].

A series of operations of the outage tables of the collection system, offshore booster station, submarine cable, and M3C station is conducted to obtain the overall available capacity table of the fractional frequency system. The raw wind speed data are subjected to clustering analysis. The power output distribution of the wind farm is calculated using a wind turbine wake-effect model. The convolution operation is performed between the output table and the overall capacity table, resulting in the distribution of the grid-connected output on the fractional frequency side:

$$p(o) = \sum_{s \in O} p_{\mathrm{s}}(s) p_{\mathrm{w}}\left(\frac{o}{s}\right) \tag{14}$$

where k is the output power of the FFTS; p_{s} is the probability distribution of the available capacity of offshore wind systems; p_{w} is the normalized turbine output distribution; s is the available capacity of offshore wind systems; and O is the system outage status set.

The analysis methods for the HVDC transmission system are similar. The difference lies in the fact that the FFTS elevates the frequency and connects to the grid through onshore M3C stations, whereas the HVDC system undergoes AC-DC conversion through offshore and onshore MMC converter stations. Extensive research has been conducted on HVDC systems and MMC converter [28], [29]; therefore, this study does not provide details.

III. Impact of Severe Weather

Wind resources directly affect the output of wind power systems. In addition, the repair processes for offshore wind power systems are related to weather factors.

Under normal circumstances, the component repair process considering severe weather conditions can be analyzed using a multistate Markov model, where the reliability parameters vary depending on the weather conditions [30], [31]. However, the Markov model does not reflect the workflow of maintenance activities and does not account for the continuity of repair work. Considering the submarine cables as an example, the maintenance process involves tasks, such as identifying fault locations, digging trenches, and conducting salvage operations within the trenches. These tasks are complex and time consuming. Maintenance vessels cannot operate at sea during severe weather. If a maintenance vessel is already at sea, it must return to the dock immediately, leading to work interruptions. Given the complex features of this maintenance process, which are closely tied to weather conditions, a direct application of the multistate model is unsuitable.

Offshore wind farms have significantly different characteristics from onshore wind farms, such as low accessibility, especially in the case of severe weather affecting access to the sea, which greatly extends the repair time of faulty components. We analyze the impact of weather from this perspective and define severe weather as conditions in which "the repair vessel is unable to go out to sea," referencing relevant studies. Specifically, severe weather is defined as conditions where "the wind speed at sea level is greater than 12 m/s and the wave height is greater than 2 m" [32], [33]. Common scenarios in the repair process can be divided into three types: normal maintenance, hold-off maintenance in severe weather, and interrupted maintenance in severe weather. These are shown in Figs.7 (a), (b), and (c).

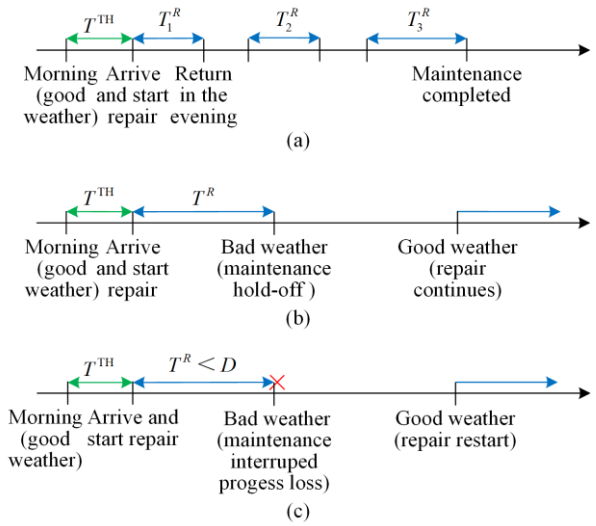

Fig. 7. Three types of repair processes. (a) Normal maintenance process. (b) Hold-off maintenance process. (c) Interrupted maintenance process.

The maintenance of offshore wind farms is commonly carried out during the daytime, and night work is generally not permitted. Maintenance work typically involves multiple procedures that can be divided into several subtasks and performed sequentially. Certain subtasks, such as robot line inspection, can be interrupted and progress saved at any time, which is defined as interruptible work. However, quitting certain tasks midway is considered invalid; for example, splicing cable sections, which is defined as non-interruptible work. The maintenance of submarine cables comprises of three subtasks: line inspection, cutting, and splicing. The first subtask is interruptible, whereas the latter two are non-interruptible. Considering that there are no restrictions on going offshore, the number of days required to complete subtask i is

$$D_i = \text{ceil}\left(\frac{T^{\text{RH}}}{T^{\text{WH}} - 2T^{\text{TH}}}\right) \tag{15}$$

where ceil( ) represents the ceiling function; T^{RH} is the net operating time required for maintenance; T^{WH} is the work time of one working day, including the travel time to and from the failure site; and T^{TH} is the travel time to the failure site.

To simplify the process analysis of completing a sub-task, we assume that the conditions for going out to sea remain fixed within a day. This means a day is either entirely work hours at sea or no work hours at all. The number of days with more than six daytime hours out of the total 12 hours is considered the count of permissible days for sailing. The original model is then transformed from an hourly time scale to a daily time scale. From the actual data, it can be observed that severe weather occurs in consecutive intervals, averaging several hours each time, which justifies this simplification. Considering severe weather as a process occurring at a constant arrival rate, it can be approximated as a Poisson process. The average arrival rate of severe weather can be used to describe this process.

Starting from the moment of failure, the distribution of the number of days that cannot be sailed within d days should follow Γ distribution. Thus, the probability of having D_{ns} non-sailable days within d days is given by the equation:

$$p(d) = \begin{cases} \dfrac{\lambda(\lambda d)^{D_{\text{ns}}-1}}{(D_{\text{ns}}-1)!}\mathrm{e}^{-\lambda d}, & d \geqslant D_{\text{ns}} \\ 0, & d < D_{\text{ns}} \end{cases} \tag{16}$$

where λ denotes the severe-weather arrival rates.

For interruptible task i, the completion condition is as follows: the last day is a good-weather day, and there are $D_i - 1$ good-weather days. The mean repair time T_i^{R} for such task i is

$$T_i^{\text{R}} = D_i p(D_i, 0) + \sum_{d=D_i}^{+\infty} (d+1)(1-\lambda) p(d, d-D_i+1) \tag{17}$$

For the non-interruptible task j, the last D_j days are guaranteed to have good weather, and the penultimate day $D_j + 1$ must have bad weather. Let the probability of bad weather be denoted as λ and the probability of good weather be denoted as $A = 1 - \lambda$. The probability of unfinished maintenance within d days, with the last day in bad weather, is calculated as follows:

$$p(d) = \lambda \quad , \quad 1 \leqslant d \leqslant D_j \tag{18}$$

recursively push the situation for the next few days:

$$\begin{cases} p(D_j+1) = \lambda A^{D_j-1} p(1) + \cdots + \lambda p(D_j) = \lambda(1 - A^{D_j}) \\ p(D_j+2) = \lambda A^{D_j-1} p(2) + \cdots + \lambda p(D_j+1) = \\ \qquad Ap(D_j+1) - \lambda A^{D_j} p(1) + \lambda p(D_j+1) \\ \qquad \cdots \\ p(i+1) = Ap(i) - \lambda A^{D_j} p(i - D_j) + \lambda p(i) \end{cases} \tag{19}$$

then the mean time T_j^{R} of non-interruptible task j is:

$$T_j^{\text{R}} = A^{D_j} D_j + \sum_{d=1}^{\infty} p(d) A^{D_j} (d + D_j) \tag{20}$$

In conclusion, taking into account the impact of severe weather on maintenance accessibility, the expression for the repair rate is as follows:

$$\mu = \frac{1}{\sum (T_i^{\text{R}} + T_j^{\text{R}})} \tag{21}$$

Summarizing the above research contents, the overall flow of the reliability assessment method is shown in Fig. 8.

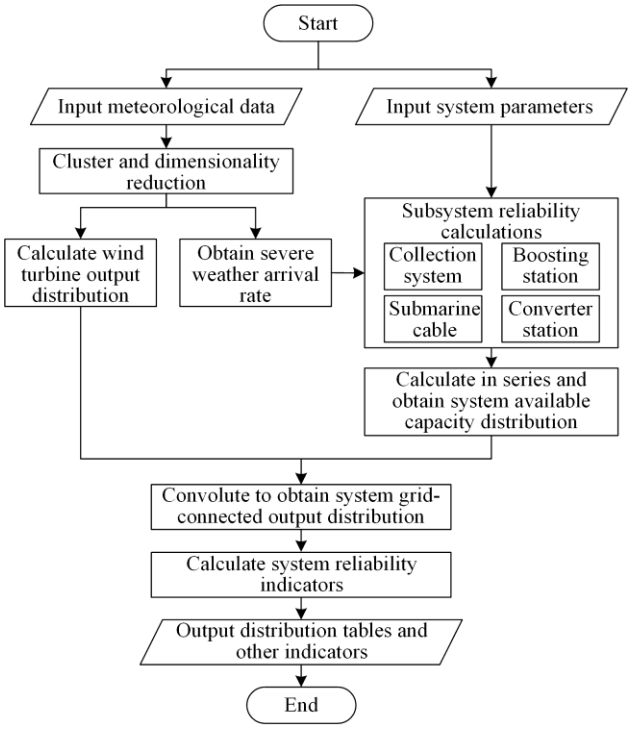

Fig. 8. Flowchart of overall reliability assessment method.

IV. Case Studies

Evaluation methods for offshore wind power system reliability mainly include the following two categories:

1) Evaluation of the output adequacy. The evaluation of the system output adequacy mainly focuses on describing the ability of the system to provide grid-connected electricity. It is a comprehensive indicator that considers both the generating capacity and reliability of offshore wind power systems and is the most direct and comprehensive reflection of the reliability of offshore wind power systems. The expected grid-connected power is an indicator for evaluating power adequacy, which reflects the main characteristics of the offshore wind power system for the grid as an equivalent power source.

2) System reliability evaluation. System reliability evaluation focuses on describing the average level of a system outage caused by component failure. Because offshore wind power systems are significantly affected by wind speed, the output reduction caused by system failures is hidden by wind speed changes, and the grid-connected output cannot clearly reflect the overall reliability of the system. The average available capacity of the system is an index for evaluating the system reliability.

Based on the aforementioned reliability assessment method, this section describes the construction of a 900 MW offshore wind power delivery system and the analysis of its reliability. Subsequently, the reliability of the systems in different sea areas, topologies, and transmission methods is evaluated and compared.

A. 900 MW Offshore Wind Power System

The fractional frequency offshore wind power system is shown in Fig. 9 and consists of three offshore wind farms, all with a capacity of 300 MW. The total capacity of the system is 900 MW with 180 wind turbines. Each wind farm adopts a linear topology with one breaker for each string of turbines, as shown in Fig. 10.

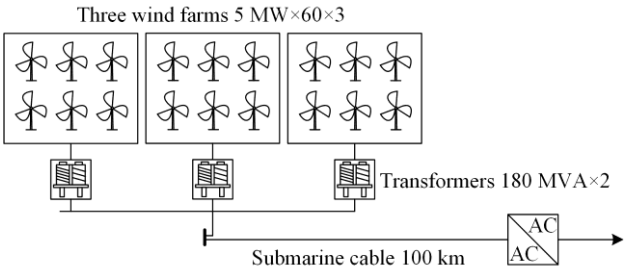

Fig. 9. Structure of FFTS case.

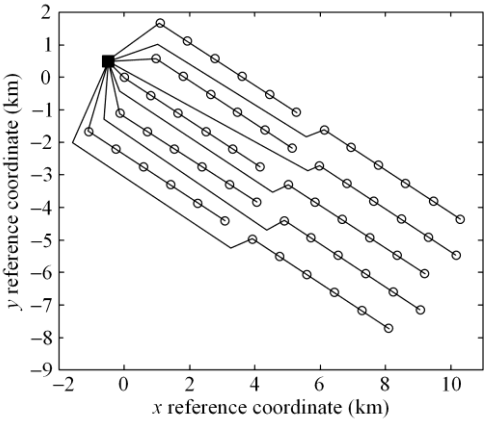

Fig. 10. Collection system with a linear topology.

The wind farm employs a converging single-bus four-section wiring configuration. Each booster station is equipped with two main transformers, each rated at 180 MVA. The length of the submarine cables is 100 km. The onshore converter station uses an M3C converter. The number of submodules of each bridge arm is 200 without considering redundancy, with 10% redundancy, and the M3C control system is not configured for backup.

Wind-speed data are extracted from the ERA5 database. This case study uses hourly wind speed data in the sea area of eastern Jiangsu, China, for a total of five years from 2018 to 2022, with coordinates of 33°N latitude and 122°E longitude. The wind speed and wind direction rise diagrams at a height of 100 m are shown in Fig. 11.

To analyze reliability, the wind speed data are first processed by K-means clustering to calculate the wind farm output distribution under the influence of a weak effect. Based on the reliability model of each subsystem described in the previous section, the system outage table and the distribution of the grid-connected output are calculated to obtain the reliability index.

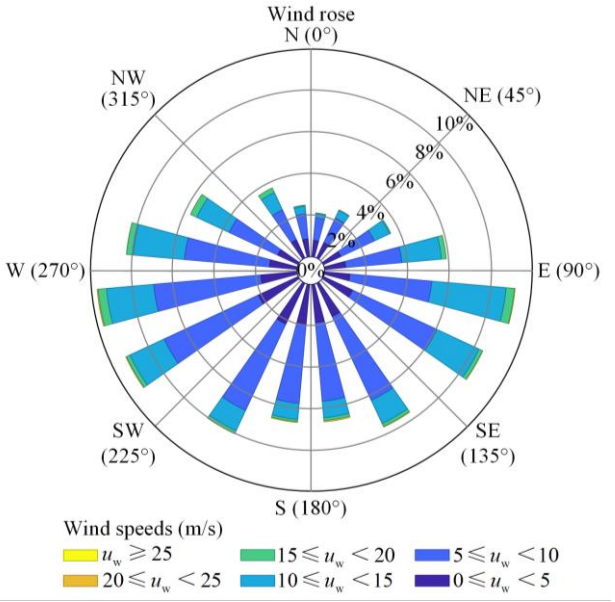

Fig. 11. Rose diagram of wind speed and direction.

The availability of the key links is listed in Table I.

TABLE I
AVAILABILITY OF KEY LINK

Link	Availability	Unavailability
Collection system	0.9656	0.0344
Converging bus	0.9954	0.0046
Boosting station	0.9985	0.0015
Submarine cable	0.9713	0.0287
M3C station	0.9701	0.0299

According to the reliability assessment results, the average availability of the overall offshore wind power system is 90.37%, the expected available capacity is 813.30 MW, the expected grid-connected output is 368.87 MW, and the annual utilization of the wind farm is 3590 h.

The system outage table and distribution of the grid-connected output are as follows:

Comparatively, the reliability of the collection system, submarine cable, and M3C station is lower because 1) under the linear structure and single breaker, the entire wind turbine string will be out of operation when any breaker or cable fails, which is less reliable; 2) the submarine cable has a high failure rate, and once it fails, the wind farm loses all power, which has a great impact on the system; and 3) the internal structure of the M3C station is complex, with many subcomponents prone to failure.

The current practical applications of FFTS are still relatively limited. Referring to the HVDC and HVAC systems from existing projects along the southeast coast of China, the average grid-connected output of offshore wind farms is approximately 1/3 of the capacity, and the actual output ratio meets the calculation results based on the model; thus, the accuracy of the model is indirectly verified.

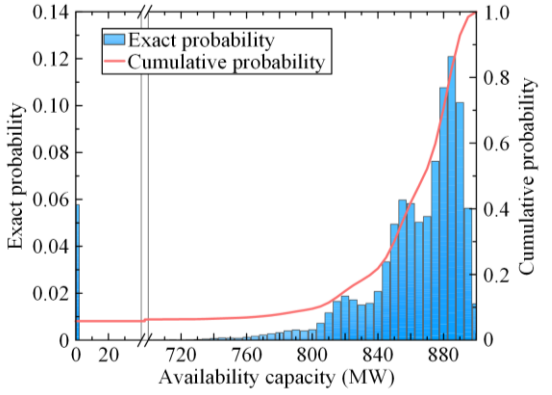

Fig. 12. Outage table of system.

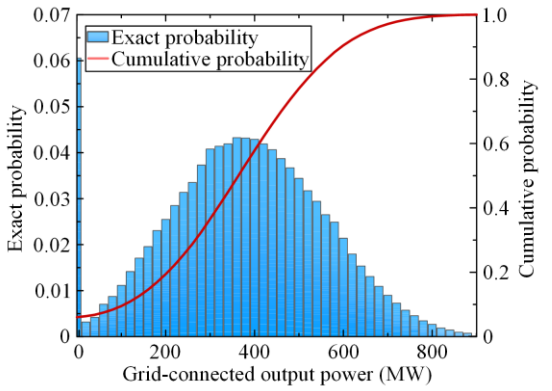

Fig. 13. Grid-connected output distribution.

B. Cases with Different System Structure

Based on the reliability model, the impact of different topologies of the system was analyzed. We consider the following three system structures:

Case1: Liner type collection system with conventionally configured breakers, a single converging bus, 5% redundancy of M3C bridge arms, and a control system without standby.

Case2: Liner type collection system with fully configured breakers, dual converging buses, 10% redundancy of M3C bridge arms, and a control system without standby.

Case3: Loop type collection system with fully configured breakers, four-section converging bus, 20% redundancy of M3C bridge arms, and control system with standby.

The structure of the loop-topology collection system is illustrated in Fig. 14.

The reliability indices of the fractional-frequency offshore wind power system under different schemes were calculated and are listed in the following table.

TABLE II
RELIABILITY INDICES FOR THREE CASES

Case	Average availability	Expected capacity (MW)	Expected output (MW)
1	0.8698	782.84	354.10
2	0.9050	814.50	369.99
3	0.9229	830.60	376.73

It can be observed that the reliability of Case1 to Case3 increases incrementally. Case3 increases the average system availability by 5.31% compared to Case1, and the grid-connected output expectation increased by 6.40%. This is mainly because 1) when the breaker configuration of the collection system is increased, a fault only needs to remove part of the turbine from the failed string; 2) the boosting station adopts a multi-segment bus, so that in the event of a failure of any bus, power can be sent from other segments through the reverse operation; and 3) the higher redundancy of M3C allows the bridge arm to withstand more sub-module failures, and when the control system of the station fails, it can be switched to the backup system to avoid station shutdown.

However, it should not be ignored that with the optimization of the system structure and an increase in the number of components, investment costs will increase, and how to strike a balance between economy and reliability remains an issue to be considered.

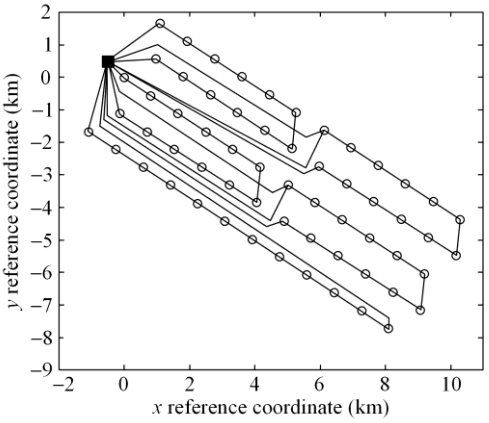

Fig. 14. Collection system with loop topology.

C. Cases with Different Transmission Methods

Among the three common offshore wind power delivery methods, the network loss and charging power of HVAC are larger, requiring the use of large-cross-section submarine cables and reactive power compensation stations. This significantly reduces the project economy and does not guarantee feasibility when the wind farm is farther away from the shore. In this study, two offshore wind power systems, the HVDC and FFTS, are compared. The parameters of the case example are the same as in Part A. Section IV shows the topology of the HVDC system, where the converter station uses an MMC converter.

The reliability indices are listed in Table III.

TABLE III
RELIABILITY INDICES OF THE TWO TRANSMISSION METHODS

Methods	Average availability	Expected capacity (MW)	Expected output (MW)
HVDC	0.8796	791.62	359.03
FFTS	0.9037	813.30	368.87

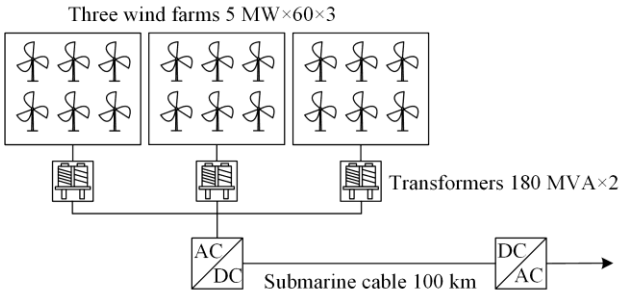

Fig. 15. Structure of HVDC case.

These results indicated that the FFTS system is more reliable than the HVDC system. This is primarily because the HVDC system requires two converter stations–onshore and offshore–whereas the FFTS system requires only onshore converters. The reliability of offshore components is low because they are more difficult to repair, and the maintenance process is affected by severe weather. After calculation, the availability of the offshore converter station is approximately 0.964 and the availability of the onshore converter station is approximately 0.979, which leads to a lower reliability of the HVDC system.

D. Cases in Different Sea Areas

To analyze the impact of environmental factors (severe weather and wind resource abundance) on the reliability of offshore wind power systems, different geographic regions are selected and their meteorological data were extracted.

The system structure is the same as that in Part A, and three sea areas are selected: the eastern sea area of Jiangsu, the southeastern sea area of Fujian, and the southern sea area of Guangdong. The specific locations are as follows:

1) Sea area of Jiangsu: 33°N latitude and 122°E longitude;

2) Sea area of Fujian: 24°N latitude and 120°E longitude;

3) Sea area of Guangdong: 21°N latitude and 113°E longitude.

These three parts of the sea are rich in offshore wind resources, close to onshore loads, and are the main target areas for China's current and future development of offshore wind power in deep and distant seas.

The calculated severe weather arrival rate, 100-meter average wind speed, and reliability indices of the offshore wind power systems are as follows:

TABLE IV
RELIABILITY INDICES OF THE THREE AREAS

Area	Severe weather rate	Average wind speed (m/s)	Expected capacity (MW)	Expected output (MW)
Jiangsu	0.1056	7.95	813.30	368.87
Fujian	0.3609	10.34	795.30	525.61
Guangdong	0.3078	7.95	800.00	390.82

The expected capacity gradually decreases as the arrival rate of bad weather increases, because severe weather makes the repair of offshore components more time-consuming. For example, it is calculated that the average repair time of the Fujian coastal submarine cables is 45.2% higher than that of the Guangdong coastal submarine cables, thus affecting the reliability of the system.

Although high winds and waves lead to lower system reliability, wind resources are more abundant, and the actual grid-connected output expectation of the offshore wind system is likely to be higher. There is still uncertainty regarding the actual grid-connected capacity and the potential for development and construction under different conditions.

V. Conclusion

Based on the topology, this study divides the fractional frequency system into subsystems, including the collection system, boosting station, submarine cable, and M3C station. Reliability models are established and the outage table of each subsystem is solved. The total outage table and grid-connected output distribution are established using the series–parallel convolution method.

Considering the impact of severe weather on the component repair process, this study divides the repair process into two categories, interruptible and non-interruptible, analyzes the average repair time of faulty components under severe weather conditions, and corrects the reliability parameters to achieve a more refined assessment.

This study compares the grid-connected capabilities of offshore wind power systems with different topologies, sea areas, and transmission methods from the perspective of reliability. The proposed method provides a reference for the development and planning of grid-connected offshore wind power systems in China.

Acknowledgment

Not applicable.

Authors' Contributions

Zhongqi Cai: project administration and supervision. Chengxiao Wei: modeling, analysis, and writing. Sui Peng: data curation and resources. Xiuli Wang: methodology and administration. All authors read and approved the final manuscript.

Funding

This work is supported by the Project "Research on Power Frequency System Planning Methods Considering the Interactive Influence of Fractional Frequency Transmission System" (No. 030400KK52220025).

Availability of Data and Materials

Not applicable.

Declarations

Competing interests: The authors declare that they have no competing financial interests or personal relationships that could have influenced the work reported in this article.

Authors' Information

Zhongqi Cai received the master of engineering degree in electrical engineering in 2017 and is currently an engineer working in the Guangdong Power Grid Corporation Zhuhai Power Supply Bureau. He has long been engaged in the research and management of new power system planning and operation control technologies.

Chengxiao Wei received the bachelor of engineering degree from the School of Electrical Engineering, Xi'an Jiaotong University in 2023 and is currently pursuing a master's degree in electrical engineering. His research interests include power system planning and reliability assessments.

Sui Peng received the master of engineering degree in Electrical Engineering in 2018 and is currently an engineer at the Guangdong Power Grid Corporation Power Grid Planning and Research Center. He has long been engaged in the research and management of offshore wind power planning and offshore wind power transmission technology.

Xiuli Wang received the B.S., M.S., and Ph.D. degrees in electrical engineering from Xi'an Jiaotong University, Xi'an China, in 1982, 1985, and 1997, respectively. Since 1985, she has been with Xi'an Jiaotong University, where she is currently a professor at the School of Electrical Engineering. Her research interests include power markets, reliability assessment of power systems, and integration of renewable power.

References

[1] P. Sherman, X. Chen, and M. McElroy, "Offshore wind: an opportunity for cost-competitive decarbonization of China's energy economy," *Science Advances*, vol. 6, no. 8, pp. 1-8, Feb. 2020.

[2] X. Wang, X. Wei, and L. Ning *et al*., "Integration techniques and transmission schemes for off-shore wind farms," *Proceedings of the CSEE*, vol. 34, no. 31, pp. 5459-5466, Nov. 2014. (in Chinese)

[3] X. Wang, "The fractional frequency transmission system," in *IEE Japan Power & Energy*, Tokyo, Japan, Jul. 1994, pp. 53-58.

[4] T. Zheng, W. Song, and W. Lü, "Asymmetric fault ride-through control strategy for a low frequency AC transmission system based on a modular multilevel matrix converter," *Power System Protection and Control*, vol. 51, no. 8, pp. 107-117, Apr. 2023. (in Chinese)

[5] X. Wang, X. Zhang, and L. Ning *et al*., "Application prospects and challenges of fractional frequency transmission system in offshore wind power integration,"

Electric Power Engineering Technology, vol. 36, no. 1, pp. 15-19, Jan. 2017.

[6] S. Zhao, C. Shao, and J. Ding *et al*., "Unreliability tracing of power systems for identifying the most critical risk factors considering mixed uncertainties in wind power output," *Protection and Control of Modern Power Systems*, vol. 9, no. 5, pp. 1-15, Sep. 2024.

[7] T. Yang and B. Shen, "Review of failure mechanism and state monitoring technology for modular multilevel converter IGBT modules," *Power System Protection and Control*, vol. 51, no. 4, pp. 174-187, Feb. 2023. (in Chinese)

[8] B. Wang, X. Wang, and B. Wang *et al*., "Reliability evaluation model and method of offshore wind power fractional frequency delivery system," *Power System Technology*, vol. 46, no. 8, pp. 2899-2908, Aug. 2022. (in Chinese)

[9] K. Luo, J. Guo, and S. Ma *et al*., "Review of key technologies of reliability analysis and improvement for offshore wind power grid integration," *Power System Technology*, vol. 46, no. 10, pp. 3691-3702, Oct. 2022. (in Chinese)

[10] I. Athamna, M. Zdrallek, and E. Wiebe *et al*., "Impact of improved models on the reliability calculation of offshore wind farms," in *Proceedings of 2014 Power Systems Computation Conference*, Wroclaw, Poland, Aug. 2014, pp. 1-7.

[11] P. Hou, W. Hu, and S. Mohsen *et al*., "Optimized placement of wind turbines in large-scale offshore wind farm using particle swarm optimization algorithm," *IEEE Transactions on Sustainable Energy*, vol. 6, no. 4, pp. 1272-1282, Oct. 2015.

[12] F. González-Longatt, P. Wall, and V. Terzija, "Wake effect in wind farm performance: steady-state and dynamic behavior," *Renewable Energy*, vol. 39, no. 1, pp. 329-338, Sep. 2011.

[13] F. Portáe-Agel, Y. Wu, and C. Chen, "A numerical study of the effects of wind direction on turbine wakes and power losses in a large wind farm," *Energies*, vol. 6, no. 10, pp. 5297-5313, Oct. 2013.

[14] J. S. Shin and J. O. Kim, "Optimal design for offshore wind farm considering inner grid layout and offshore substation location," *IEEE Transactions on Power System*, vol. 32, no. 3, pp. 2041-2048, May 2017.

[15] G. Abeynayake, T. V. Acker, and D. V. Hertem *et al.*, "Analytical model for availability assessment of large-scale offshore wind farms including their collector system," *IEEE Transactions on Sustainable Energy*, vol. 12, no. 4, pp. 1974-1983, Oct. 2021.

[16] B. Wang, X. Wang, and X. Wang *et al*., "Reliability evaluation of wind plant considering collector grid," *Proceedings of the CSEE*, vol. 35, no. 9, pp. 2105-2111, May 2015. (in Chinese)

[17] P. Lakshmanan, R. Sun, and J. Liang, "Electrical collection systems for offshore wind farms: a review," *CSEE Journal of Power and Energy Systems*, vol. 7, no. 5, pp. 1078-1092, Sep. 2021.

[18] S. Liu, X. Wang, and Y. Meng *et al*., "A decoupled control strategy of modular multilevel matrix converter for fractional frequency transmission system," *IEEE Transactions on Power Delivery,* vol. 32, no. 4, pp. 2111-2121, Aug. 2017.

[19] C. Wang, Z. Zheng, and K. Wang *et al*., "Analysis and control of modular multilevel matrix converters under branch fault conditions," *IEEE Transactions on Power Electronics*, vol. 37, no. 2, pp. 1682-1699, Feb. 2022.

[20] P. Tu, S. Yang, and P. Wang. "Reliability- and cost-based redundancy design for modular multilevel converter," *IEEE Transactions on Industrial Electronics*, vol. 66, no. 3, pp. 2333-2342, Mar. 2019.

[21] B. Wang, X. Wang, and Z. Bie *et al*., "Reliability model of MMC considering periodic preventive maintenance," *IEEE Transactions on Power Delivery*, vol. 32, no. 3, pp. 1535-1544, Jun. 2017.

[22] J. Guo, X. Wang, and J. Liang *et al*., "Reliability modeling and evaluation of MMCs under different redundancy schemes," *IEEE Transactions on Power Delivery*, vol. 33, no. 5, pp. 2087-2096, Oct. 2018.

[23] C. A. Arbugeri, S. A. Mussa, and M. L. Heldwein, "AC-AC modular multilevel converter-hexverter," *Energies*, vol. 15, no. 22, Oct. 2022.

[24] Y. Meng, B. Liu, and H. Luo *et al*., "Control scheme of hexagonal modular multilevel direct converter for offshore wind power integration via fractional frequency transmission system," *Journal of Modern Power Systems and Clean Energy*, vol 6, no. 1, pp. 168-180, Jan. 2017.

[25] M. Nakamura, N. Nanayakkara, and H. Hatazaki *et al*., "Reliability analysis of submarine power cables and determination of external mechanical protections," *IEEE Transactions on Power Delivery*, vol. 7, no. 2, pp. 895-902, Apr. 1992.

[26] M. Bawart, M. Marzinotto, and G. Mazzanti, "A deeper insight into fault location on long submarine power cables," *Elektrotechnik & Informationstechnik*, vol. 131, no. 8, pp. 355-360, Dec. 2014.

[27] C. Shen, X. Wang, and Q. Zhang *et al*., "Reliability model of submarine cable based on time-varying failure rate," *Distribution & Utilization*, vol. 38, no. 5, May 2021.

[28] Y. Song, Y. Luo, and X. Xiong, "Loss distribution analysis and accurate calculation method for bulk-power MMC," *Protection and Control of Modern Power Systems*, vol. 8, no. 4, pp. 1-14, Oct. 2023.

[29] Y. Guo, H. Gao, and Q. Wu, "A combined reliability model of VSC-HVDC connected offshore wind farms considering wind speed correlation," *IEEE Transactions on Sustainable Energy*, vol. 8, no. 4, pp. 1637-1646, Oct. 2017.

[30] L. Li, Y. Sun, and Y. Huang, "Reliability evaluation of offshore wind farm and VSC-HVDC integrated system considering the influence of extreme weather," *Southern Power System Technology*, vol. 14, no. 12, pp. 32-42, Dec. 2020.

[31] Z. Lu, L. Cheng, and Y. Qiao *et al*., "Offshore wind power system reliability evaluation considering wind resource constraints and double weather patterns," *Power System Technology*, vol. 39, no. 12, pp. 3536-3542, Dec. 2015. (in Chinese)

[32] L. Huang, Y. Fu, and Y. Mi *et al*., "A Markov-chain·-based availability model of offshore wind turbine considering accessibility problems," *IEEE Transactions on Sustainable Energy*, vol. 8, no. 4, pp. 1592-1600, Oct. 2017.

[33] S. Mahmood, "Maintenance logistics organization for offshore wind energy: current progress and future perspectives," *Renewable Energy*, vol. 77, pp. 182-193, May 2015.